EFFECT OF SINTERING TEMPERATURE ON MICROSTRUCTURE AND ELECTRICAL PROPERTIES OF ZnO + CaMnO$_3$ CERAMICS USED IN LOW-VOLTAGE VARISTORS

I. I. LAKIN[a], A. ZAKARIA[b*], Y. ABDOLLAHI[c], D. UMARU[d]

[a]Department of Physics, Faculty of Science, Universiti Putra Malaysia, 43400 UPM Serdang, Selangor, Malaysia
[b]Department of Physics, Faculty of Science, Universiti Putra Malaysia, 43400 UPM Serdang, Selangor, Malaysia
[c]Materials Synthesis and Characterization Laboratory, Institute of Advanced Technology, Universiti Putra Malaysia, 43400 UPM Serdang, Selangor, Malaysia
[d]Department of Physics, Faculty of Science, Universiti Putra Malaysia, 43400 UPM Serdang, Selangor, Malaysia

In the study, the effect of sintering temperature on microstructure and electrical properties of low voltage varistor ceramics prepared from ZnO doped with CaMnO$_3$ perovskite (CMO) and sintered at 1200 to 1320 °C was investigated. The initial powder of the ceramics was prepared from 5 mol% CMO synthesized by coprecipitation processing and ZnO powder. The sintered discs of the mixed powders were analyzed by using TG/DTG, XRD, VPSEM and EDX. The disc density decreased from 5.24 to 5.15 g/cm^3 and its average grain size increased in the range of 6.68 – 10.87 μm, while the breakdown voltage increased in the range of 90.2 to 135.4 V/mm with increase of sintering temperatures. The varistor ceramics highest nonlinear coefficient of 37.2 was obtained at 1300 °C sintering temperature with minimal leakage current of 23.7 μA/cm^2.

1. Introduction

Zinc oxide (ZnO) based low voltage varistors as semiconducting ceramics devices have been widely used in electronic circuits and electrical power systems for protection against unwanted over-voltage surges. The ceramic is produced by sintering of ZnO powder with small amounts of additives in the varistor due to its highly nonlinear current-voltage characteristics and energy handling capabilities [1, 2]. The nonlinear characteristics are attributed to the formation of double schottky barriers at the ZnO grain boundaries in the microstructure of the ceramics. The nonlinear current density-electric field (*J-E*) characteristics are expressed by $J = KE^{\alpha}$, where K is a constant and α is the nonlinear coefficient that is originated from the microstructure, precisely the ZnO grain size [3-6]. Therefore, the nonlinearity heavily depends on the microstructure; thus, grain size and microstructural homogeneity are the most significant parameters in varistor processing[7]. The inhomogeneous microstructures easily suffer from a deviation of the nonlinear characteristics due to high local currents and over loads from single large grains, which results in rapid degradation of the varistor in electronics and electrical systems [8-10]. The sintering process for ZnO varistor ceramics gives rise to a distinctive microstructure, which consist of semiconducting *n*-type ZnO grains surrounded by very thin insulating intergranular layers.

Sintering is an essential step in the preparation of ZnO varistor ceramics. Sintering is influenced by various factors, such as sintering time, sintering temperature, heating rate, cooling rate and sintering methods, which directly affects the microstructure of ZnO varistor ceramics, as

---

* Corresponding author: azmizak@gmail.com

well as grain size, uniformity of grains and boundary structure thereby, affecting its electrical properties, such as varistor voltage E_b, α, and resistivity impact [11-17]. Microstructure and electrical properties are important factors that can be adjusted by the means of sintering temperature[18]. The improvement of electrical properties and microstructure of varistor ceramic are achieved by adding impurities such as Sb_2O_3, Bi_2O_3 or by thermal annealing. However, Sb_2O_3 – free varistors with good characteristics are now in demand owing to its toxicity, Bi_2O_3 also has its setback such as high volatility and reactivity [19-21]. On the other hand, perovskite manganite $AMnO_3$, where A is an alkaline earth metal such as Ca, Sr, Ba and Pb, has been the subject of intense research during the last decade due to their unique properties that make them attractive in enhancing the performance of the existing materials [22]. The perovskite show the unusual property of being paramagnetic insulators at high temperatures and ferromagnetic metals at low temperatures. The partial doping of the divalent alkaline earth cation by trivalent rare earth ion leads to the formation of a mixed valence state of the manganese, Mn^{3+} and Mn^{4+} to maintain the charge neutrality of the system [23-25]. ZnO ceramics doped with perovskite phases $M^1 M^2 O_{3-x}$ less than 2 mol % as the only forming additive exhibits good α greater than 45. Here M^1 is a multivalent transition-metal ion such as Mn, Cu and Co, and M^2 is an alkaline earth or rare-earth ion with larger radius and more electropositive than Zn such as Ca, Ba and La [26]. In addition, the optimization of the non-stoichiometric conventional additives is very difficult while $CaMnO_3$-added ZnO ceramics microstructure is simple consisting of only ZnO grain and $CaMnO_3$ (CMO) as intergranular layer [27]. In this present work, the effect of sintering temperature on microstructure and electrical properties of low voltage varistor ceramics fabricated from a mixture of 5 mol % CMO perovskite prepared by chemical coprecipitation and 95 mol % ZnO powders were studied. The precursor powder was studied via TG/DTG, ceramic discs were investigated using XRD, VPSEM, EDX analysis, and *J-E* characteristic measurement.

2. Experimental Procedure

2.1 Materials

Starting raw materials with composition ratio of 5 mol % CMO + 95 mol % ZnO used as reagent-grade materials for ZCMO-based varistors. ZnO powder with particle size ≤ 1 μm with 99.9 % purity (Sigma Aldrich) was selected as the host material. Manganese acetate $(Mn(C_2H_3O_2)_2)$ with 98 % purity (Sigma Aldrich) and calcium acetate monohydrate $(Ca(C_2H_3O_2).H_2O)$ with 98 % purity (Sigma Aldrich) were used as metal salt precursors and citric acid anhydrous with 99.5 % purity (Alpha Aesar) served as the complexing agent.

2.2 Sample preparation

Molar ratio of manganese acetate, citric acid anhydrous and calcium acetate monohydrate was 1: 2: 1. Two separate beakers containing deionized water were used to dissolve citric acid anhydrous mixed with manganese acetate, and citric acid mixed with calcium acetate monohydrate for 10 minutes duration at 70 °C with vigorous stirring to have an improved contact. Their contents were mixed in a single beaker and more deionized water was added up to 200 ml, followed by the introduction of ZnO powder to the mixture. The mixing process was prolonged at 90 °C until the liquid dried up. The cake that was left eventually was dried in an oven at 110 °C for 19 hrs. The dried cake was pulverized to produce powder with particle size < 100 μm, and then calcined at 750 °C for 2 hrs at heating and cooling rate of 2 °C/min. Later, a 1.75 wt % of polyvinyl alcohol was added to it, granulated by sieving 200-mesh screen to produce starting powder. The powder was pressed into discs of 1.1 mm diameter and 1.4 mm thickness using Specac Hydraulic Press machine. The discs were then sintered at various temperatures of 1200, 1250, 1300 and 1320 °C for 3 hrs at a heating and cooling rates of 3 °C/min. The sintered discs were lapped and polished to 7 mm in diameter and 0.8 mm thickness.

2.3 Methods of Characterizations

For electroding, both sintered disc surfaces were coated with silver conductive paint. For *J-E* characteristics it was measured by using source measure unit (Keithly 236) with the applied dc voltage from 0 – 100 V in step size of 2.0 V. The α was determined from,

$$\alpha = \frac{\log J_2 - \log J_1}{\log E_2 - \log E_1} \tag{1}$$

where E_1 and E_2 are the electric fields corresponding to current densities $J_1 = 1.0$ and $J_2 = 10$ mA cm^{-2}, respectively. The breakdown voltage, E_b was determined as the corresponding E at $J = 1$ mA cm^{-2} while the leakage current density was determined as the corresponding J at $E = 0.85E_b$. Voltage per grain boundary, V_{gb} was determined from $E_b d/D$ where d is the average grain size calculated using lineal intercept method, D is the disc thickness. For phase identification of the sintered samples using XRD (PANalytical (Philips) X$^{'}$ pert Pro PW3040/60) with Cu*K*α source. Sample was radiated with Ni-filtered CuKα radiation (λ = 1.5428) within 2θ scan range of 20-80 °C. The grain distributions and microstructure of the samples were studied using Vapor Pressure Scanning Electron Microscope (VPSEM) integrated with EDX. Thermogravimetry and differential thermal analysis (TG/DTA) was done using TGA/DSC-1 Mettler Toledo for examining the thermal decomposition profile of the precursor powder. The sample was heated from 30-900 °C in air at 10 °C min^{-1}.

3. Results and discussion

3.1 The ceramic core Microstructure

Figure 1 shows the XRD patterns of sintered ZnO doped with CMO at all temperatures (1200, 1250, 1300 and 1320 °C) for 3 hrs sintering time. The patterns confirmed the presence of dominant ZnO phase (ICDS reference code 00-036-1451) and CMO (ICDS reference code 00-050-1746) with the presence of Ca$_3$ZnMnO$_6$ (ICDS code 01-089-4556) as secondary phase, formed at the grain boundaries (spectrum 1) and the triple point junction (spectrum 2) as observed from EDX (Figure 3). This is due to the Mn^{2+} ions which have larger ionic radii compared to Zn^{2+} segregated at the grain boundaries as secondary phases. However this phase reduces when the sintering temperature was increased to 1300 °C due to the reactive melting of CMO leading to the formation of phase with complete wettability and excellent interface coherence on ZnO leading to stable heterostructures [28].
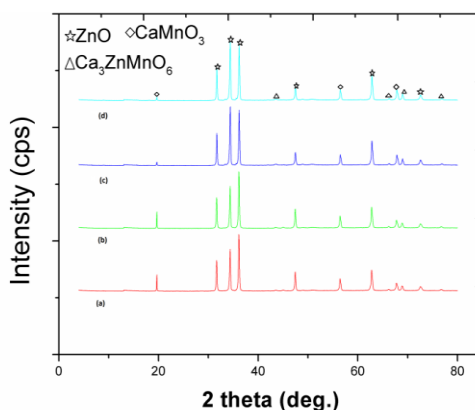

Fig. 1 XRD patterns of the samples for various sintering temperatures:
(a) 1200 °C, (b) 1250 °C, (c) 1300 °C and (d) 1320 °C.

Figure 2 shows SEM micrographs of the ZnO-CMO system for various sintering temperature. The grain structure is nonuniformly distributed throughout the samples. However, with increasing sintering temperature, this nonuniformity was significantly reduced. All the samples show uniform equiaxed grains and free from abnormal grain growth, where the grain growth of the ZnO is promoted by CMO doping and rounded corners of the grain shape is observed. The overall trend in the grain growth is increasing as the sintering temperature increases. Moreover, it can be easily seen that the grain boundaries are clearer as the sintering temperature increased.
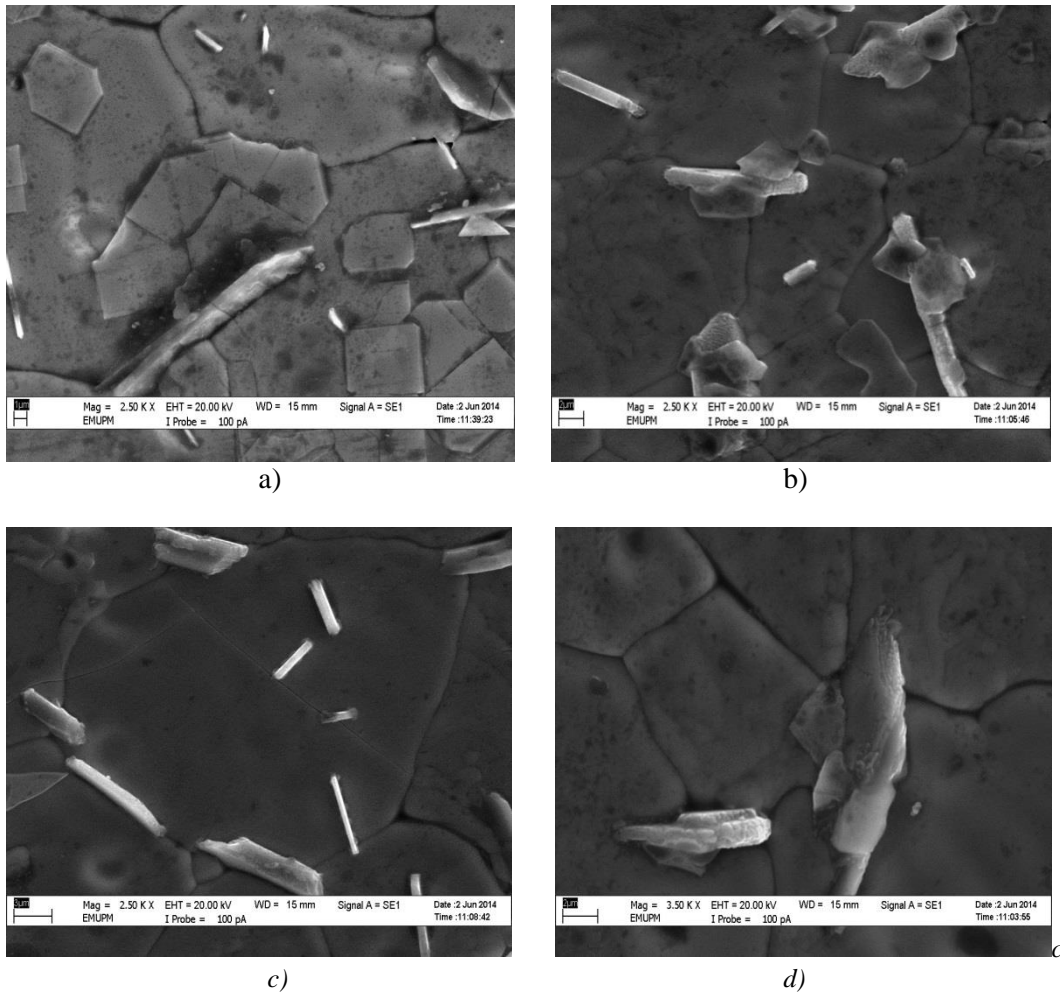

a)

b)

c)

d)

Fig. 2 VPSEM micrographs of varistor ceramics for various sintering temperatures:
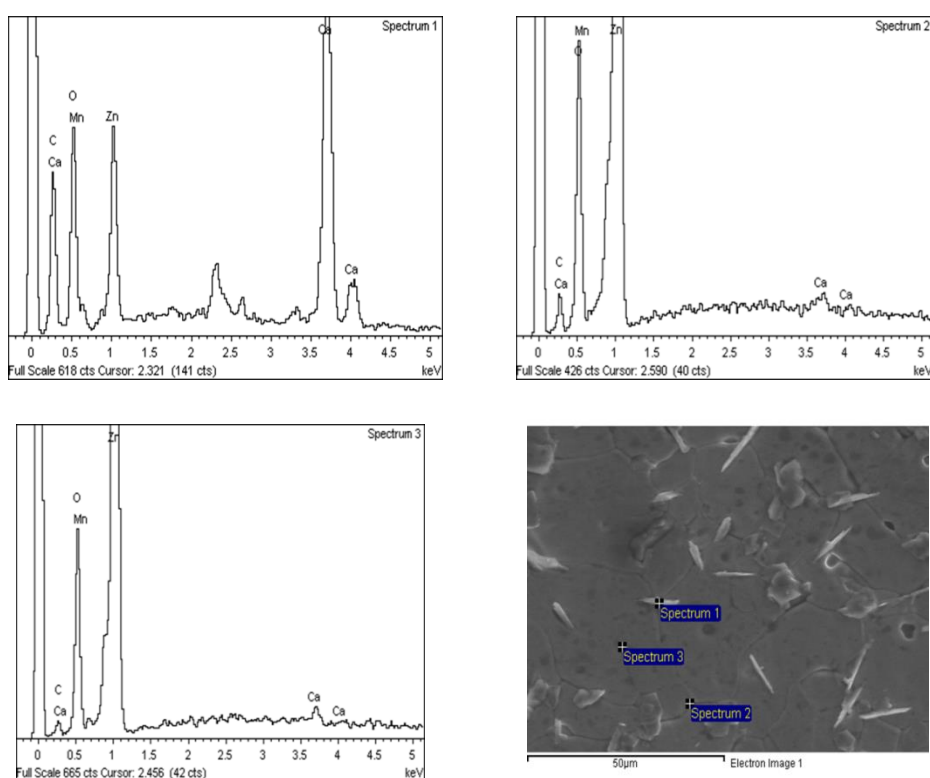*(a) 1200 °C (b) 1250 °C (c) 1300 °C and (d) 1320 °C.*

*Fig. 3 VPSEM micrograph of polished surface for sintered ceramic at 1300 °C
and its corresponding EDX analysis.*

Figure 4 shows the thermal decomposition profile of CMO powder and ZnO doped with CMO. From Figure 4(a), the weight loss peaks at 175, 233, 420, 681 and 903 °C, respectively shows the major steps in which the pure CMO powder decomposed. The first step within the range of 123-210 °C was associated to the removal of moisture. The second step in the range of 210-379 °C was related to the decomposition of excess citric acid. The third step ranging from 380-591 °C was also associated with the formation of intermediate phases such as carbonates or oxides. The continuous weight loss between 593-720 °C was assigned to the gradual decomposition of carbonates to oxides from the Ca and Mn gel mixture. Figure 4(b) shows the decomposition of ZnO-CMO powder at 3 different steps at 101, 357 and 647 °C respectively. The first step was associated with moisture evaporation. While the second steps was linked to the elimination of excess citric acid. The last step was attributed to the decomposition of carbonates. Therefore, better quality of ZnO-CMO would be achieved at calcination temperature above 650 °C.
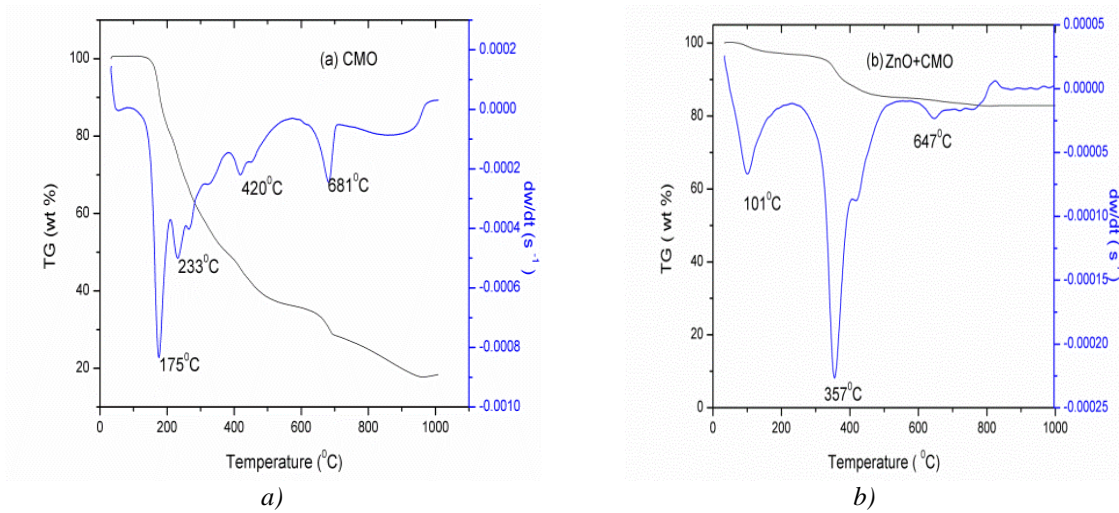
Fig. 4 TG/DTA curves of (a) CMO powder and (b) ZnO-CMO powder heated in air at heating rate of 10 °C/min.

3.2 Electrical Characterization

Figure 5 shows the *J-E* characteristics of the samples for various sintering temperatures. The curves are divided into two regions: one is a non-ohmic region with extremely low impedance after breakdown field and another is an ohmic region with extremely high impedance before breakdown field. The sharper the knee of the curve between the two regions the better the varistor properties. It can be seen from the curves that the sintering temperature has a significant effect on the varistor properties. The detailed *J-E* characteristics parameters are summarized in Table 1.

Table 1 Microstructure and electrical parameters of the samples for various sintering temperatures

Sintering temperature (°C)	d (μm)	ρ (g/cm^3)	E_b (*V*/mm)	V_{gb} (V)	α	J_L (μA/cm^2)
1200	6.68	5.24	90.2	0.7	16.3	69.5
1250	7.94	5.22	129.5	1.3	23.1	43.3
1300	10.07	5.17	131.1	1.1	37.2	23.7
1320	10.87	5.15	135.4	1.7	27.4	26.8

The breakdown field (E_b) linearly increased from 90.2 to 135.4 *V*/mm with increasing sintering temperature. The varistor sintered at 1200 °C provided low varistor voltage per thickness of the ceramics. This is very important for low voltage varistor. The increase of E_b with increasing sintering temperature is attributed firstly to the decrease in the number of grain boundaries caused by the increase in the ZnO grain size and secondly, the abrupt increase of varistor voltage per grain boundaries (V_{gb}). α also linearly increased from 16.3 to 37.2 with the increase of sintering temperature up to 1300 °C. However, further increase in sintering temperature caused α to decrease to 27.4 at 1320 °C. As a result it can be seen that the sintering temperature has a significant effect on the nonlinear properties in the light of α variation.
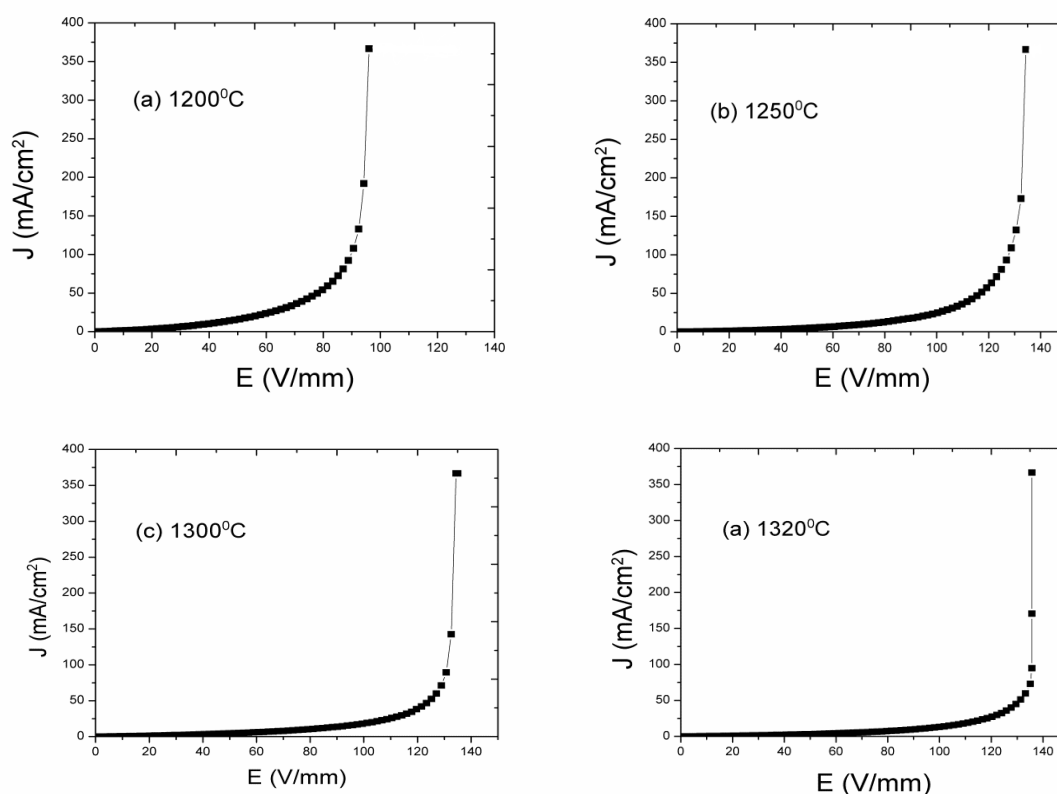
Fig. 5 J-E characteristics of samples for various sintering temperatures.

The behavior of α in accordance with sintering temperatures, temperature can be related to the variation of Schottky barrier height according to the variation of the electronic states at the grain boundaries. The sintering temperature will vary the density of the interface states with transport of the defect ions toward the grain boundaries. Therefore, the decrease of α in accordance with sintering temperature is attributed to the decrease in potential barrier height at the grain boundaries. E_b exhibited high values compared with other low-voltage varistor ceramics.

The variation of α against sintering temperature is depicted in Figure 5. α is enhanced when sintering temperature increased from 1200 to 1300 °C which suggests that segregation of CMO in grain boundary has promoted the development of needed potential barrier at interface. However, as the sintering temperature increased to 1320 °C the value of α decreased due to the decrease of recombination current between electrons and holes in the vicinity of the grain boundaries

The variation of α against sintering temperature is depicted in Figure 6. Here, α is enhanced when sintering temperature increased from 1200 to 1300 °C which suggests the segregation of CMO in grain boundary has promoted the development of needed potential barrier at interface. However, as the sintering temperature increases to 1320 °C α decrease due to the decrease of recombination current between electrons and holes in the vicinity of the grain boundaries [1]. On the other hand as the sintering temperature increased, the leakage current (J_L) value decreased achieving a minimum value 23.7 μA/cm^2 for the ZCMO ceramics sintered at 1300 °C. Increasing sintering temperature further to 1320 °C caused J_L increased to 20μA/cm^2. This is attributed to the reduction of barrier height [28]. It was observed that, as the sintering temperature increased, the density of the sintered ceramics was decreased from 5.24 to 5.15 g/cm^3.
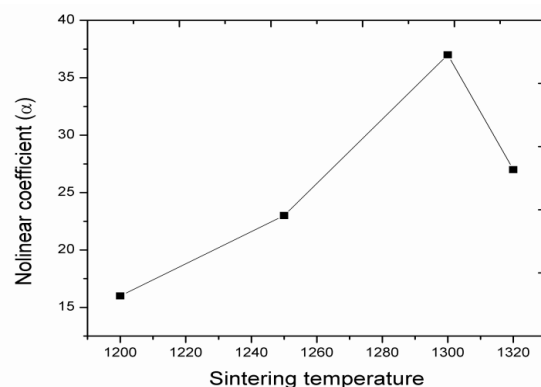
Fig. 6 Variation of α against sintering temperature.

4. Conclusion

The effect of sintering temperature on ZnO-CMO based ceramics was investigated in the range of 1200 to 1320 °C. The sintering temperature influences the microstructure and nonlinear properties of the ceramics. The XRD and EDX analysis of the samples show presence of primary phases ZnO, CMO and Ca_3ZnMnO_6 as a minor secondary phase. Analysis from TG/DTG revealed that better quality of ZnO-CMO would be achieved at calcination temperature above 650 °C. Result from VPSEM showed that the average size of the ZnO grain increased (6.68-10.87 μm) with the increase in sintering temperature. It can be seen that α initially increases and then decreases with the increase in sintering temperature. The ceramics sintered at 1300 °C exhibited the highest value of α of 37.2, while the ceramics sintered at 1200 °C is the least having 16.3 as α. The leakage current J_L showed an opposite trend to that of α value where J_L decreased as sintering temperature increase. The breakdown field E_b increased in the range of 90.2 to 135.4 V/mm and a preferential segregation of CMO dopants at grain boundaries was improved with the increase in sintering temperature.

References

[1] D.R. Clarke, Journal of the American Ceramic Society **82**, 485 (1999).
[2] M.-H. Wang, C. Yao, N.-F. Zhang, Journal of Materials Processing Technology **202,** 406 (2008).
[3] R.K. Sendi, A. Munshi, S. Mahmud, Superlattices and Microstructures **69**, 212 (2014).
[4] C.-W. Nahm, Ceramics International **39**, 3417 (2013).
[5] H. Zhou, R. Guo, D. Chu, B. Chang, Y. Qin, L. Fang, Journal of Materials Science: Materials in Electronics **24**, 4987 (2013).
[6] R.K. Sendi, A. Munshi, S. Mahmud, Superlattices and Microstructures **69**, 212 (2014).
[7] M. Takada, S. Yoshikado, Journal of the European Ceramic Society **30**, 531 (2010).
[8] E. Olsson, G. Dunlop, R. Österlund, Journal of the American Ceramic Society **76**, 65 (1993).
[9] M.E. Abrishami, A. Kompany, S. Hosseini, N.G. Bardar, Journal of Sol-gel Science and Technology **62**, 153 (2012).
[10] S. Hingorani, D. Shah, M. Multani, Journal of Materials Research **10**, 461 (1995).
[11] X. Liu, K. Pan, W. Li, D. Hu, S. Liu, Y. Wang, Ceramics International (2014).

[12] M. Gao, X. Wu, J. Liu, W. Liu, Applied Surface Science **257**, 6919 (2011).

[13] C.W. Nahm, Journal of the American Ceramic Society **93**, 2297 (2010).

[14] C.-W. NAHM, Ceramics International **35**, 2679 (2009).

[15] C.-W. Nahm, Materials Science and Engineering: B **136**, 134 (2007).

[16] C.-W. Nahm, Journal of Materials Science: Materials in Electronics **20**, 418 (2009).

[17] A. Sedky, T. El-Brolossy, S. Mohamed, Journal of Physics and Chemistry of Solids **73**, 505 (2012).

[18] W.-S. Lee, W. Chen, Y. Lee, T. Yang, C. Su, C. Hu, Ceramics International **33**, 1001 (2007).

[19] J. Fan, R. Freer, Journal of Materials Science **28**, 1391 (1993).

[20] Y.S. Lee, T.Y. Tseng, Journal of the American Ceramic Society **75**, 1636 (1992).

[21] C.-W. Nahm, Journal of the European Ceramic Society **23**, 1345 (2003).

[22] J. Dormann, D. Fiorani, Magnetic properties of fine particles, Elsevier, 1992.

[23] S. Nakamura, Y. Tadokoro, Y.J. Shan, T. Nakamura, Journal of the Physical Society of Japan **68**, 1485 (1999).

[24] J. Philip, T. Kutty, Materials Chemistry and Physics **63**, 218 (2000).

[25] K. Vijayanandhini, T. Kutty, Journal of Materials Science: Materials in Electronics **20**, 445 (2009).

[26] N. Raghu, T. Kutty, Applied Physics Letters **60**, 100 (1992).

[27] K. Vijayanandhini, T. Kutty, Applied Physics Letters **88**, 123513 (2006).

[28] C.-W. Nahm, Materials Letters **60**, 3394 (2006).